Terahertz Spin Precession and Coherent Transfer of Angular Momenta in Magnetic Quantum Wells

S. A. Crooker,[1] J. J. Baumberg,[2] F. Flack,[3] N. Samarth,[3] and D. D. Awschalom[1]

[1]*Department of Physics, University of California, Santa Barbara, California 93106*
[2]*Hitachi Cambridge Laboratory, Madingley Road, Cambridge CB3 0HE, United Kingdom*
[3]*Department of Physics, Pennsylvania State University, University Park, Pennsylvania 16802*

Femtosecond-resolved measurements of induced Faraday rotation reveal exchange coupling between the spin angular momenta of charge carriers and a sublattice of magnetic ions in semiconductor quantum wells. In transverse magnetic fields, we observe terahertz spin precession of photoinjected electrons, rapid spin relaxation of holes, and the coherent transfer of angular momentum to the magnetic sublattice via the ultrafast rotation of the local moments. The perturbed ions undergo free-induction decay, enabling time-domain all-optical electron-spin-resonance measurements in single magnetic planes. [S0031-9007(96)01291-4]

Recent interest in magnetic semiconductor heterostructures is strongly driven by the large spin-dependent energy splittings of carriers which arise from enhanced exchange interactions with localized magnetic ions [1]. In addition to revealing the physics of low-dimensional and quantum-confined spin systems through spectroscopy, the resulting spin-polarized energy states are potentially relevant for spin transport and related spin-effect devices. It has also been demonstrated in recent years that the strong coupling between carriers and local moments allows one to follow the temporal variation of exciton spin states by enabling the magnetic tuning of electronic energy levels simultaneously with time-resolved spin-sensitive spectroscopies [2–4]. In such experiments, the evolution of an optically prepared exciton spin population is monitored through a time-dependent optical response. In contrast, more conventional probes of spin dynamics in condensed matter systems such as pulsed nuclear magnetic resonance (NMR) record the precession of local moments after a perturbing impulse, yielding detailed information about the local magnetic environment. Here we present analogous optical experiments in magnetic semiconductor heterostructures that help disentangle the interactive spin dynamics of electrons, holes, and magnetic moments in quantum confined geometries.

We have utilized an ultrafast optical Faraday rotation technique in which the applied magnetic field $(\vec{H}\|\hat{x})$ responsible for aligning the magnetic Mn^{2+} ions is perpendicular to both the growth axis of a quantum well structure and to the photoinjected carrier spins $(\vec{S}\|c\|\hat{z})$. The strong s-d exchange interaction between the electron spins and the embedded Mn^{2+} ions amplifies the frequency of electron spin precession about the magnetic field, yielding field-tunable THz oscillations in the measured $\hat{z}$ component of spin. In contrast the hole spins scatter rapidly, making it possible to distinguish the spin relaxation of both electrons and holes in a range of applied fields and temperatures and identify the enhancement from magnetic

scattering. The transient hole exchange field rotates the net magnetization of the Mn^{2+} ions $(\vec{M}^{Mn})$ away from the applied field axis. This *coherent* magnetic perturbation, akin to a tipping pulse in NMR, is followed by an oscillatory free-induction decay of the Mn^{2+} moments, persisting long after the carriers have decayed. This phenomenon enables all-optical spin-resonance measurements of magnetic ions in quantum geometries.

The molecular-beam-epitaxy- (MBE-) grown samples are 120 Å $Zn_{0.77}Cd_{0.23}Se/ZnSe$ single quantum wells (QWs) on ⟨100⟩ GaAs having different local concentrations of Mn^{2+} ions. Three are digital structures, in which a fixed total amount of MnSe [3 monolayers (ML)] is incorporated into the well in a series of equispaced planes, allowing direct control over the average distance and coupling between neighboring Mn^{2+} spins [2]. The QWs contain a single 3-ML barrier of MnSe (1×3 ML), three equispaced single monolayers of MnSe (3×1 ML), 24 one-eighth ML ($24 \times 1/8$ ML), or a nonmagnetic control (NM). A fifth sample contains a single 4-ML barrier of $Zn_{0.90}Mn_{0.10}Se$ (4 ML 10%). The growth rates of the various components of the heterostructures are determined to within 5% using *in situ* electron diffraction studies. X-ray diffraction studies of corresponding multilayer samples indicate that the interdiffusion profile has a relatively narrow width (~1 ML) during growth, giving local quasi-2D Mn^{2+} concentrations of 100%, 50%, 8%, and 10%, respectively [2]. The samples exhibit narrow (~6 meV) heavy-hole (hh) exciton absorption peaks and g factors in longitudinal field at $T = 4.6$ K ranging from 2 (NM) to 430 ($24 \times 1/8$ ML) due to strong sp-d exchange and increased spatial overlap between the magnetic ions and the photoexcited carrier wave functions.

The samples are mounted in a magneto-optical cryostat in transverse fields $(\vec{H}\|\hat{x})$, aligning the Mn^{2+} moments along the plane of the quantum well [inset, Fig. 1(a)]. Spin-polarized electrons and holes, initially oriented normal to the plane of the well $(\vec{S}^{e,h}\|\hat{z})$, are optically injected
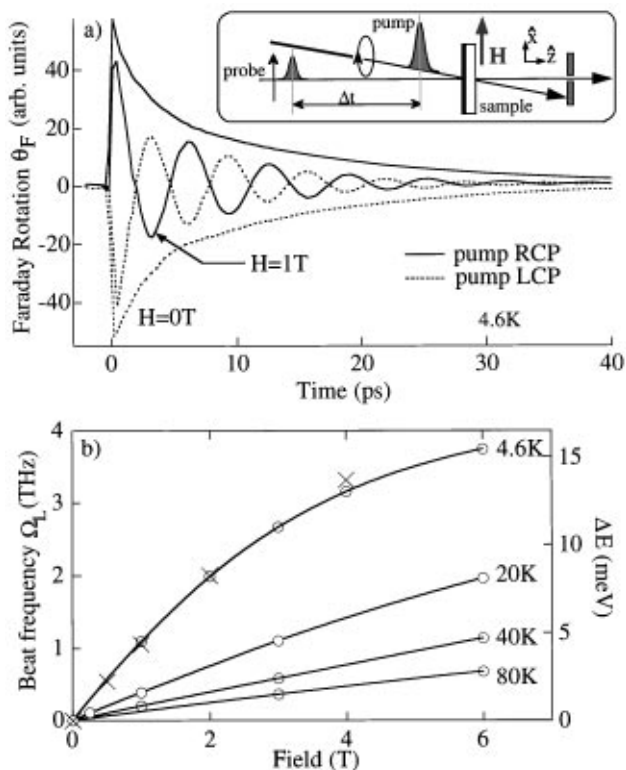
FIG. 1. (a) Pump-induced Faraday rotation, measuring net carrier spin $\langle S_z \rangle$, in transverse fields $H = 0$, 1 T for pumping with right (solid) and left (dashed) circularly polarized light in the quantum well containing the 4-ML $Zn_{0.90}Mn_{0.10}Se$ barrier. Inset: Schematic of experiment. Pump/probe polarizations are as drawn. (b) Electron precession frequency and corresponding electron Zeeman splitting at 4.6 K in the $24 \times 1/8$ ML sample vs applied field. Crosses are exciton splitting scaled down by factor 5.7.

by 120 fs pump pulses of circularly polarized light tuned to the peak of the hh resonance. The net magnetization of the sample parallel to $\hat{z}$ is measured via the Faraday rotation imparted to a weak, time-delayed, linearly polarized probe pulse. An optical polarization bridge measures the pump-induced changes in the Faraday rotation of the probe with submillidegree sensitivity [3].

Figure 1(a) shows the Faraday rotation following injection of spin-polarized electrons ($S_z^e = \pm\frac{1}{2}$) and holes ($S_z^h = \mp\frac{3}{2}$) into the 4 ML 10% magnetic quantum well. The Faraday rotation on these short time scales reflects the component of net carrier spin oriented along the $\hat{z}$ axis and displays the expected reversal of sign upon pumping with the opposite sense of circular polarization. In zero applied field, the observed superposition of two exponential decays arises from the spin relaxation of the electrons and holes, which then recombine on a longer time scale. As discussed below, the hole spins relax quickly (<5 ps) in these zinc-blende structures despite the removal of the light hole-heavy hole degeneracy by strain, while electron spin scattering is significantly slower. Similar behavior has been predicted and observed in unstrained GaAs quan-

tum wells, with the rapid hole spin relaxation attributed to valence band mixing [5,6].

This monotonic behavior is significantly modified upon application of a transverse magnetic field, H_x. Pronounced oscillations appear in the measured Faraday rotation resulting from the precession of the net electron spin $\langle S_z^e \rangle$ about the orthogonal field, $B_x = \mu_0(H_x + M_x^{Mn})$. This field-tunable Larmor precession frequency can be several THz in magnetic semiconductor systems due to the strong s-d exchange between the conduction band and the local Mn^{2+} spins. The electrons are quantized along the field axis ($S_x^e = \pm\frac{1}{2}$), thus photoinjecting electron spins with definite S_z^e corresponds to pumping a coherent superposition of the spin-split electron states $\pm S_x^e$. This superposition "beats" at the frequency determined by the electron Zeeman splitting, $\Delta E = g_{eff}^e \mu_B H_x$. Consequently, the Larmor frequency $\Omega_L = \Delta E / \hbar$ directly provides the effective g factor g_{eff}^e and spin-splitting ΔE of the electrons alone, as recently found in luminescence experiments on nonmagnetic GaAs [7]. Figure 1(b) shows the field dependence of Ω_L and ΔE in the $24 \times 1/8$ ML sample at different temperatures. As expected, Ω_L tracks the magnetization of the sample, which follows a Brillouin function arising from the alignment of the paramagnetic Mn^{2+} spins [8]. Also shown is the corresponding *exciton* Zeeman splitting, reduced by a factor of 5.7, as measured by the spin splitting of the hh exciton absorption peaks in longitudinal magnetic fields [2]. These data clearly support identification of the precession signal as arising from the electrons alone—reflectivity measurements in bulk $Zn_{1-x}Mn_xSe$ indicate nearly the same ratio (5.8) between exciton and electron g factors [9].

At early times the measured Faraday rotation is fit well by the sum of an exponentially decaying cosinusoidal oscillation (electrons) and a faster purely exponential decay [Fig. 2(a)], which we identify with the rapid spin relaxation of the photoinjected hole population. The holes do not precess; their angular momenta are constrained to lie along the growth axis ($c \parallel \hat{z}$) due to strain and quantum confinement [10], resulting in a vanishing hh spin splitting in transverse magnetic fields (for $B < 8$ T). This ability to clearly differentiate between the evolution of the net electron and hole spin enables a detailed study of the role of applied field and magnetic environment upon the individual population's spin relaxation. In zero field, samples with larger overlap between the carrier wave functions and embedded magnetic ions (3 $\times$ 1 ML, $24 \times 1/8$ ML) show more rapid spin scattering of both electrons (τ_s^e) and holes (τ_s^h) [Figs. 2(b) and 2(c)]. This is likely due to alloy-induced fluctuations in the potential landscape induced by local magnetic scattering centers [11]. In a field, hole longitudinal scattering rates in the magnetic samples are enhanced, reflecting strong magnetically mediated scattering.

The electron oscillations are directly analogous to the free-induction decays of transverse nuclear spin which
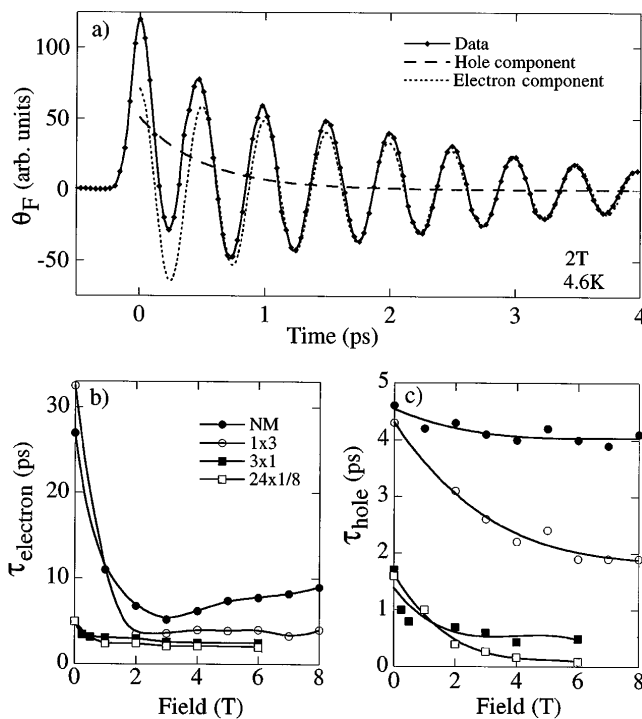
FIG. 2. (a) Induced Faraday rotation (solid) in the $24 \times 1/8$ ML sample, showing the rapid initial decay of the holes superimposed on the electron precession. (b),(c) Decay times of the electron oscillations (τ_s^e) and the hole component (τ_s^h) vs field at $T = 4.6$ K for the digital structures indicated. Lines are guides to the eye.
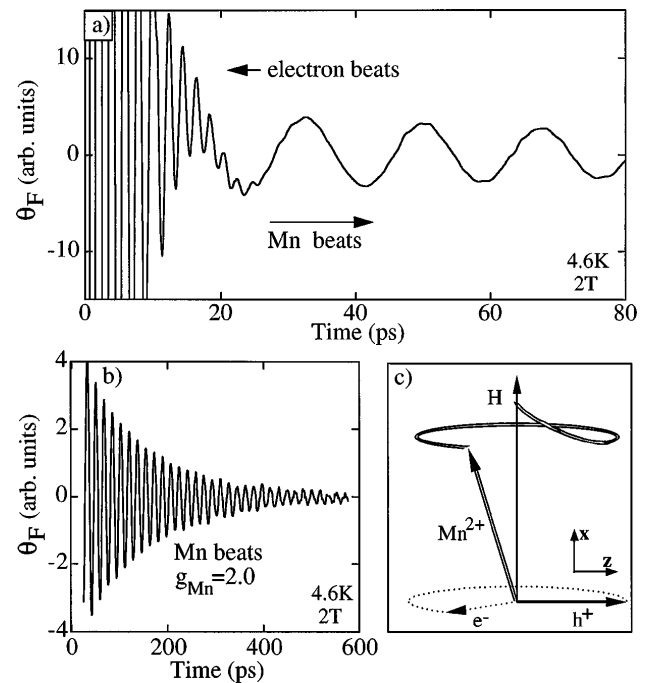

FIG. 3. (a) Induced Faraday rotation, showing the final oscillations of the electrons superimposed on an induced precession of the Mn spins in the sample containing the 4 ML $Zn_{0.90}Mn_{0.10}Se$ barrier. (b) Evolution of the Mn precession, showing long-lived free-induction decay. (c) Diagram of the initial coherent rotation of the Mn spins caused by the hole exchange field.

follow a 90° tipping pulse in NMR. In applied fields, we measure a transverse spin relaxation T_2^* of the photoinjected electrons which is related to the longitudinal spin relaxation time (T_1) and the homogeneous dephasing time (T_2') in magnetic resonance by the relation $1/T_2^* \cong 1/2T_1 + 1/T_2'$. While the precise contribution from the two effects is still under investigation, it is clear that the increase in the spin relaxation rate with field is much larger for those samples with little or no coupling to the Mn moments. In contrast to data drawn from the Hanle effect, these measurements provide a direct and simple temporal characterization of spin scattering and offer a new method of time-domain electron spin resonance in undoped semiconductor quantum structures.

The utility of the Faraday rotation technique lies in its ability to measure induced sample magnetizations that persist long after the injected carriers have recombined. Figure 3(a) shows the final decay of the electron precession in the 4 ML 10% sample and reveals a surprising result: There remains an additional oscillation, persisting for hundreds of picoseconds [Fig. 3(b)], with a period and decay time implying the free induction of coherent Mn^{2+} spins. The photoexcited carriers have imparted a net transverse magnetization $\langle \Delta M_z^{Mn} \rangle$ to the ensemble of local moments, which subsequently and collectively precess at microwave frequencies about the applied field. The signal reverses sign with opposite circular pump, while the precession frequency scales linearly with applied field, is sample and

temperature independent (2–100 K), and corresponds to that expected for $g_{Mn} = 2.0$. The observed decay time of these magnetic oscillations agrees well ($\pm 10\%$) with ESR measurements of the dephasing time (T_2^{Mn}) of Mn^{2+} spins in bulk $Zn_{0.90}Mn_{0.10}Se$ [12], confirming the realization of an all-optical time-domain spin-resonance experiment that is easily capable of probing small numbers of spins.

A possible mechanism for initiating the observed spin-resonance signal lies in the impulsive coherent rotation of Mn^{2+} moments about the transient exchange field ($H_{exch} \| \hat{z}$) generated by the hole spins. To first order, the electrons can be excluded from consideration, since any contribution averages away due to their much faster precession. The sample magnetization $\vec{M}^{Mn}$, oriented initially along the applied field H_x, is rotated away from the $\hat{x}$ axis upon application of a torque $\| \hat{y}$ by the strong exchange field of the holes, which persists for the hole spin relaxation time, acting on each ion [Fig. 3(c)]. A similar process has been invoked to explain Raman data in magnetic semiconductor quantum wells, where up to 15 Mn spin-flip Stokes lines are observed [13]. After the holes equilibrate, the perturbed Mn moment, which has been rotated by up to a half degree from the x axis in these experiments, then precesses freely. Strong evidence for this mechanism is seen from extrapolating the Mn beats back to zero delay, which shows the oscillations build up sinusoidally as predicted in this model. The effect of the hole exchange field is directly analogous to the

radio-frequency tipping pulses used in NMR studies to initiate free-induction decays in nuclear moments.

We rule out two other scenarios by which transverse angular momentum may be imparted to the Mn sublattice, namely, by direct spin-flip scattering between the hole spins and the Mn spins or by a polaronic effect in which the Mn moments align with S_z^h. The former case would yield a net long-lived magnetic signal even in zero applied field, which we have never observed in any sample (the Mn beat amplitude tends to zero as the field is decreased to zero). In addition, Mn beats triggered by scattering should preserve angular momentum $\| \hat{z}$ and thus have a maximum amplitude at zero delay in disagreement with the data. As for the latter scenario, no direct evidence of polaron formation is seen in dc or time-resolved optical spectra. In addition, polaron formation is known to occur over much longer time scales ($\sim 50-100$ ps) [14], over an order of magnitude longer than the rapid (<5 ps) transfer of angular momenta that our data would indicate.

We use this optical generation and detection of free-induction decays in the embedded Mn^{2+} ions to explore the spin resonance of diluted magnetic planes. Figure 4(a) shows the temperature-dependent dephasing times (T_2^{Mn}) of the Mn moments for varying spatial distributions. The variation of T_2^{Mn} with temperature and spin distribution is in qualitative agreement with exchange narrowing models [15], which relate the transverse relaxation time
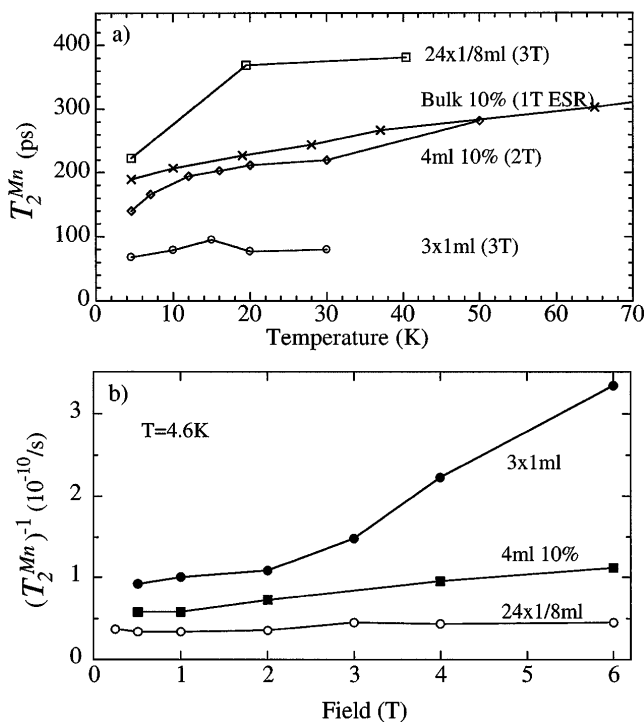
to anisotropic and isotropic spin-spin interactions, as well as to static and dynamic spin-spin correlations. Note that while the $24 \times 1/8$ ML sample and the 3×1 ML sample contain an identical number of Mn spins the different local spin densities ($\sim 8\%$ and $\sim 50\%$) are clearly evidenced in their disparate decay times (230 and 70 ps at 4.6 K and 3 T), highlighting the crucial role of nearest-neighbor spin-spin interactions in determining the transverse relaxation process. An important difference between the all-optical ESR measurement carried out here and conventional frequency domain ESR is the capability of continuously measuring the variation of T_2^{Mn} with magnetic field. For instance, at low temperatures, the Mn spin dephasing rate $(T_2^{Mn})^{-1}$ increases dramatically with field for the sample with the highest local Mn density [Fig. 4(b)]. Such a field dependence of the relaxation time may be responsible for the anomalous non-Lorentzian ESR line shapes observed in bulk magnetic semiconductors with high Mn concentration at low temperatures [15].

FIG. 4. (a) Temperature dependence of the Mn transverse spin relaxation time for samples with different local Mn concentrations. Also shown ($\times$) are ESR measurements of the Mn dephasing time in bulk $Zn_{0.90}Mn_{0.10}Se$ from [12]. (b) Field dependence of the Mn spin relaxation rate for samples with different local Mn densities.

[1] D. D. Awschalom and N. Samarth, in *Optics of Semiconductor Nanostructures,* edited by F. Hennenberger and S. Schmitt-Rink (Akademie Verlag, Berlin, 1993).

[2] S. A. Crooker *et al.*, Phys. Rev. Lett. **75**, 505 (1995).

[3] J. J. Baumberg *et al.*, Phys. Rev. B **50**, 7689 (1994); S. A. Crooker *et al.*, IEEE J. Sel. Top. Quantum Electron. **1**, 1082 (1995).

[4] T. Östreich, K. Schönhammer, and L. J. Sham, Phys. Rev. Lett. **74**, 4698 (1995); **75**, 2554 (1995).

[5] S. Bar-Ad and I. Bar-Joseph, Phys. Rev. Lett. **68**, 349 (1992); T. C. Damen *et al.*, Phys. Rev. Lett. **67**, 3432 (1991).

[6] T. Uenoyama and L. J. Sham, Phys. Rev. Lett. **64**, 3070 (1990); R. Ferreira and G. Bastard, Phys. Rev. B **43**, 9687 (1991).

[7] A. P. Heberle *et al.*, Phys. Rev. Lett. **72**, 3887 (1994); M. Oestreich and W. W. Rühle, Phys. Rev. Lett. **74**, 2315 (1995).

[8] *Diluted Magnetic Semiconductors*, edited by J. K. Furdyna and J. Kossut (Academic, San Diego, 1988).

[9] A. Twardowski *et al.*, Solid State Commun. **48**, 845 (1983).

[10] R. W. Martin *et al.*, Phys. Rev. B **42**, 9237 (1990); B. Kuhn-Heinrich and W. Ossau, in *II-VI Compounds and Semimagnetic Semiconductors,* edited by H. Heinrich and J. B. Mullin (Trans. Tech. Publications, Switzerland, 1995).

[11] R. Hellman *et al.*, *II-VI Compounds and Semimagnetic Semiconductors* (Ref. [10]).

[12] S. Rajagopalan, Ph. D. thesis, Purdue University, 1988.

[13] J. Stühler *et al.*, Phys. Rev. Lett. **74**, 2567 (1995).

[14] D. D. Awschalom *et al.*, Phys. Rev. Lett. **66**, 1212 (1991); G. Mackh *et al.*, Phys. Rev. B **50**, 14 069 (1994).

[15] N. Samarth and J. K. Furdyna, Phys. Rev. B **37**, 9227 (1988); D. L. Huber, Phys. Rev. B **31**, 4420 (1985).